

# Thermomagnetic convection in a ferrofluid layer exposed to a time-periodic magnetic field

P. Matura and M. Lücke

*Institut für Theoretische Physik, Universität des Saarlandes, D-66041 Saarbrücken, Germany*  
 (Received 27 April 2009; revised manuscript received 14 July 2009; published 21 August 2009)

We have investigated the influence of a time-periodic and spatially homogeneous magnetic field on the linear stability properties and on the nonlinear response of a ferrofluid layer heated from below and from above. A competition between stabilizing thermal and viscous diffusion and destabilizing buoyancy and Kelvin forces occurs. Floquet theory is used to determine the stability boundaries of the motionless conductive state for a harmonic and subharmonic response. Full numerical simulations with a finite difference method were made to obtain nonlinear convective states. The effect of low- and high-frequency modulation on the stability boundaries as well as on the nonlinear oscillations that may occur is investigated.

DOI: [10.1103/PhysRevE.80.026314](https://doi.org/10.1103/PhysRevE.80.026314)

PACS number(s): 47.55.pb, 47.65.Cb, 47.20.Bp, 47.20.Ky

## I. INTRODUCTION

The spontaneous formation of spatial and temporal patterns can be observed in many physical, chemical, and biological systems that are driven out of thermal equilibrium [1]. If the driving—characterized by a control parameter—exceeds a critical threshold a structured system state grows out of an unstructured homogeneous state, thereby breaking at least one symmetry of the former state.

A well known and extensively investigated hydrodynamic pattern forming system is the Rayleigh-Bénard system [2] of a horizontal fluid layer that is heated from below and cooled from above. The control parameter is the dimensionless Rayleigh number  $Ra$ , which is a measure of the buoyancy force  $F_b \sim g\Delta T$ .  $g$  is the gravitational acceleration and  $\Delta T$  the applied temperature difference across the layer. If  $Ra$  is above the critical value  $Ra_c$ , the motionless fluid layer loses its stability against small perturbations and convection starts in the form of straight parallel rolls as they occur, e.g., in narrow channels with roll axes perpendicular to the long side walls.

The effect of time-periodic forcing, i.e.,  $Ra = Ra(t)$ , on both the onset of convection and the convective response has been investigated in some detail [3–6]. The forcing can be realized by varying the temperature difference  $\Delta T(t)$  or the gravitational acceleration  $g(t)$ . For the latter the convection cell has to oscillate, and the range of accessible amplitudes and frequencies has its limitations in the experimental setup. Considering magnetic fluids offers an alternative method to investigate periodic forcing.

Magnetic fluids (ferrofluids) show a strong paramagnetic behavior if exposed to an external magnetic field [7,8]. Their magnetization depends on the fluid temperature, which causes magnetization gradients if temperature gradients are present. This leads to destabilizing Kelvin forces, the strength of which is characterized by the dimensionless magnetic Rayleigh number  $N$ . Periodic forcing can be realized by periodic modulation of the external magnetic field which results in a time-dependent magnetic Rayleigh number  $N(t)$ . The system under consideration shows paradigmatically the response of a pattern forming system when the driving is periodically swept over the threshold.

The first theoretical investigation of the linear stability of the quiescent ferrofluid layer in the presence of a spatially

homogeneous, stationary magnetic field was made by Finlayson [9]. Qualitative experimental validations of his results were obtained by Schwab *et al.* [10]. Huang *et al.* [11] investigated the effect of a uniform oblique magnetic field and a nonuniform magnetic field [12] on the linear stability properties. Kaloni *et al.* [13] considered the convective instability problem taking the Brownian relaxation mechanism into account. In a subsequent paper they expanded their analysis to alternating magnetic fields [14]. Aniss *et al.* [15] have also studied the effect of a time-periodic magnetic field on the linear stability properties, but only for low Prandtl number fluids.

The present paper complements the linear stability considerations of [14,15]. In addition, we show for the first time nonlinear convective states of the full nonlinear governing equations, investigating the effect of the modulation on the nonlinear response. The paper is organized as follows: in Sec. II we present the system, the boundary conditions and the ground state. The linear stability analysis is performed in Sec. III including the results for high- and low-frequency modulation. The nonlinear convective states are presented in Sec. IV. We close with the summary in Sec. V. Subharmonic response is shortly discussed in the Appendix.

## II. SYSTEM

We consider a laterally periodic ferrofluid layer in the Rayleigh-Bénard setup. We apply a constant vertical temperature gradient and a spatially homogeneous external magnetic field  $\mathbf{H}_{\text{ext}}$  normal to the fluid layer (see Fig. 1). The hydrodynamic field equations (Oberbeck-Boussinesq approximation) and the magnetostatic Maxwell equations read [8,16–18]

$$\nabla \cdot \mathbf{u} = 0 \quad (2.1)$$

$$(\partial_t + \mathbf{u} \cdot \nabla) \mathbf{u} = -\nabla p + \nu \nabla^2 \mathbf{u} + \alpha g \delta T \mathbf{e}_z + \frac{\mu_0}{\rho_0} (\delta \mathbf{M} \cdot \nabla) \delta \mathbf{H} \quad (2.2)$$

$$(\partial_t + \mathbf{u} \cdot \nabla) \delta T = \kappa \nabla^2 \delta T \quad (2.3)$$

$$\nabla \cdot \delta \mathbf{B} = \mu_0 \nabla \cdot (\delta \mathbf{H} + \delta \mathbf{M}) = 0 \quad (2.4)$$

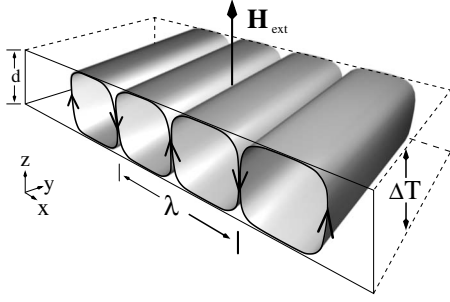


FIG. 1. Schematic setup of the Rayleigh-Bénard system with straight convection rolls with axes oriented in the  $y$  direction. A constant vertical temperature gradient  $\Delta T/d$  and a spatially homogeneous external magnetic field  $\mathbf{H}_{\text{ext}}$  normal to the fluid layer is applied. The lateral periodicity length is  $\lambda$ .

$$\nabla \times \delta \mathbf{H} = 0 \rightarrow \nabla \Phi = \delta \mathbf{H} \quad (2.5)$$

for the velocity field  $\mathbf{u} = u\mathbf{e}_x + w\mathbf{e}_z$  of straight rolls with axes oriented in the  $y$  direction, the deviations of the temperature field  $\delta T = T - T_0$ , the magnetic field  $\delta \mathbf{H} = \mathbf{H} - \mathbf{H}_0$ , and the fluid magnetization  $\delta \mathbf{M} = \mathbf{M}(\mathbf{H}, T) - \mathbf{M}_0(\mathbf{H}_0, T_0)$ .  $T_0$  denotes the mean temperature of the fluid layer,  $\mathbf{H}_0$  the magnetic field inside the isothermal fluid layer with the temperature  $T_0$ , and  $\mathbf{M}_0$  the associated magnetization of the fluid. Here,  $p$  is the pressure field,  $\nu$  the kinematic viscosity [19],  $\alpha$  the thermal expansion coefficient,  $g$  the gravitational acceleration,  $\mathbf{e}_z$  the unit vector normal to the plates,  $\mu_0$  the magnetic field constant, and  $\kappa$  the thermal diffusivity. Furthermore,  $\mathbf{B}$  is the magnetic induction and  $\Phi$  the magnetic potential.

We consider a magnetic field, which is normal to the plates, uniform in space and harmonic in time. The internal field for the isothermal fluid layer with temperature  $T_0$  is then

$$\mathbf{H}_0 = [H_S + H_M \cos(\Omega t)]\mathbf{e}_z \quad (2.6)$$

with  $H_S$  being the time averaged, static contribution of the driving,  $H_M$  the modulation amplitude, and  $\Omega$  the modulation frequency.

For the magnetization  $\mathbf{M}$  we assume the equilibrium magnetization

$$\mathbf{M}(\mathbf{H}, T) = \frac{\mathbf{H}}{H} M(H, T) = \frac{\mathbf{H}}{H} M(H/T), \quad (2.7)$$

since the vorticity of the convection is small and the period of the magnetic field modulation is much larger than the typical time scales of magnetization relaxation (Brown and Néel).

We expand  $\delta \mathbf{M}$  in a Taylor series up to linear order in  $\delta \mathbf{H}$  and  $\delta T$

$$\delta \mathbf{M} = \begin{pmatrix} \bar{\chi} & 0 & 0 \\ 0 & \bar{\chi} & 0 \\ 0 & 0 & \chi \end{pmatrix} \delta \mathbf{H} - K \delta T \mathbf{e}_z. \quad (2.8)$$

Here  $\bar{\chi} = \frac{M_0}{H_0}$  is the chord susceptibility,  $\chi = \frac{\partial M}{\partial H} \Big|_{H_0, T_0}$  the tangential susceptibility, and  $K = -\frac{\partial M}{\partial T} \Big|_{H_0, T_0} = \frac{H_0}{T_0} \chi$  the pyromagnetic coefficient. In this work we consider small magnetic fields so that  $\bar{\chi} = \chi$  is equal to the initial susceptibility.

Using Eq. (2.8), we nondimensionalize the Eqs. (2.1)–(2.5) by scaling length by the height  $d$  of the layer, time by the thermal diffusion time  $\tau_{\text{th}} = d^2/\kappa$ , temperature by the applied temperature difference  $\Delta T$  and the magnetic potential by  $d \frac{\Delta T}{T_0} \frac{\chi}{1+\chi} |\mathbf{H}_0|$

$$\nabla \cdot \mathbf{u} = 0 \quad (2.9)$$

$$(\partial_t + \mathbf{u} \cdot \nabla) \mathbf{u} = -\nabla p + \text{Pr} \nabla^2 \mathbf{u} + \text{Pr} \text{Ra} \delta T \mathbf{e}_z - \text{Pr} N \delta T \partial_z \nabla \Phi \quad (2.10)$$

$$(\partial_t + \mathbf{u} \cdot \nabla) \delta T = \nabla^2 \delta T \quad (2.11)$$

$$\nabla^2 \Phi = \partial_z \delta T. \quad (2.12)$$

We get the following dimensionless parameters: the Prandtl number  $\text{Pr} = \frac{\nu}{\kappa}$ , the Rayleigh number

$$\text{Ra} = \frac{\alpha g d^3}{\kappa \nu} \Delta T \quad (2.13)$$

and the magnetic Rayleigh number

$$N = \mu_0 \frac{\Delta T^2 d^2 \chi^2}{T_0^2 \eta \kappa (1 + \chi)} [H_S + H_M \cos(\Omega t)]^2. \quad (2.14)$$

It is useful to define additionally the time-independent control parameters

$$N_M = \mu_0 \frac{\Delta T^2 d^2 \chi^2}{T_0^2 \eta \kappa (1 + \chi)} H_M^2, \quad N_S = \mu_0 \frac{\Delta T^2 d^2 \chi^2}{T_0^2 \eta \kappa (1 + \chi)} H_S^2. \quad (2.15)$$

We also use the reduced relative Rayleigh number

$$\epsilon = \frac{\text{Ra}}{\text{Ra}_c^0} - 1 \quad (2.16)$$

with  $\text{Ra}_c^0$  being the critical Rayleigh number in the absence of magnetic fields.

### A. Boundary conditions

We consider rigid and perfectly heat conducting plates so that

$$\delta T|_{z=\pm 1/2} = \mp \frac{1}{2}, \quad w|_{z=\pm 1/2} = 0 = u|_{z=\pm 1/2}. \quad (2.17)$$

The continuity of the normal component of  $\mathbf{B}$  and the tangential component of  $\mathbf{H}$  at the interface of the magnetic fluid layer and the nonmagnetic plates implies

$$\partial_z \hat{\Phi}_m|_{z=\pm 1/2} = \mp \frac{|mk|}{1 + \chi} \hat{\Phi}_m \Big|_{z=\pm 1/2} \mp \frac{1}{2} \delta_{m,0} \quad (2.18)$$

with  $\delta_{m,0}$  being the Kronecker delta. Here  $\hat{\Phi}_m(z, t)$  denotes the  $m$ th lateral Fourier coefficient of an expansion of the magnetic potential  $\Phi(x, z, t) = \sum_m \hat{\Phi}_m(z, t) e^{imkx}$  with wave number  $k$ . We refer to these realistic boundary conditions as RBC.

For an analytical treatment, we also consider free-slip boundaries at the plates and the limit  $\chi \rightarrow \infty$

$$\begin{aligned} \delta T|_{z=\pm 1/2} &= \mp \frac{1}{2}, \quad w|_{z=\pm 1/2} = 0 = \partial_z u|_{z=\pm 1/2}, \\ \partial_z \Phi|_{z=\pm 1/2} &= \mp \frac{1}{2}. \end{aligned} \quad (2.19)$$

We refer to these idealized boundary conditions as IBC.

### B. Conductive state

The quiescent, conductive solution of Eqs. (2.9)–(2.12) reads

$$\mathbf{u}_{\text{cond}} = 0, \quad \delta T_{\text{cond}} = -z, \quad \Phi_{\text{cond}} = -\frac{1}{2}z^2. \quad (2.20)$$

The time dependence of the magnetic potential  $\Phi_{\text{cond}}$  for periodic modulation is hidden in  $|\mathbf{H}_0(t)|$  used in the scaling.

## III. LINEAR STABILITY ANALYSIS

For IBC we expand the deviations  $w$ ,  $\theta = \delta T - \delta T_{\text{cond}}$  and  $\phi = \Phi - \Phi_{\text{cond}}$  from the conductive state of the vertical velocity, the temperature field and the magnetic potential, respectively, as follows:

$$[w, \theta, \phi] = \sum_{m,n} [w_{mn}(t), \theta_{mn}(t), \phi_{mn}(t)] e^{imkx} cs(n\pi z). \quad (3.1)$$

In the lateral direction we use Fourier modes with periodicity length  $\lambda = 2\pi/k$ ,  $k$  being the associated wave number. In the vertical direction an orthogonal set  $cs(n\pi z)$  matching the boundary conditions Eq. (2.19) is used. For the  $w$  and the  $\theta$  field,  $cs$  is an abbreviation for the function *cosine* for  $n$  odd and *sine* for  $n$  even, respectively. For the  $\phi$  field, the role of *cosine* and *sine* is interchanged.

Linearizing the Eqs. (2.9)–(2.12) for the deviations, we obtain a system of decoupled second-order equations for the amplitudes  $\theta_{mn}(t)$

$$\ddot{\theta} + \Gamma \dot{\theta} = -\frac{\partial}{\partial \theta} V(\theta) \quad (3.2)$$

with

$$V(\theta) = -\frac{1}{2} \text{Pr} \tilde{q}^4 [\hat{\epsilon} + \hat{N}_S + 2\sqrt{\hat{N}_S \hat{N}_M} \cos(\Omega t) + \hat{N}_M \cos^2(\Omega t)]. \quad (3.3)$$

Here we have omitted the indices  $mn$  and introduced

$$\tilde{q}^2 = n^2 \pi^2 + m^2 k^2, \quad \Gamma = \tilde{q}^2 (1 + \text{Pr}), \quad \text{Ra}_{\text{stab}} = \frac{\tilde{q}^6}{m^2 k^2}, \quad (3.4)$$

$$N_{\text{stab}} = \frac{\tilde{q}^8}{m^4 k^4}, \quad \hat{\epsilon} = \frac{\text{Ra}}{\text{Ra}_{\text{stab}}} - 1, \quad \hat{N}_M = \frac{N_M}{N_{\text{stab}}}, \quad \hat{N}_S = \frac{N_S}{N_{\text{stab}}}. \quad (3.5)$$

The conductive solution is linearly stable, if none of the amplitudes  $\theta_{mn}(t)$  is able to grow in time, otherwise it is unstable. The growth behavior of the amplitudes depends on the details of the potential  $V$  Eq. (3.3) and on the damping  $\Gamma$ . First we briefly review the results for time independent driving (Sec. III A), then we proceed with the results for time dependent forcing (Sec. III B).

### A. Stationary magnetic fields ( $H_M = 0$ )

For stationary magnetic fields, the stability boundary of the conductive state against a perturbation with amplitude  $\theta_{mn}$  is given by the condition  $\hat{\epsilon} + \hat{N}_S = 0$  for which the curvature of the potential  $V$  Eq. (3.3) becomes zero. The critical Rayleigh number as a function of the magnetic Rayleigh number  $N_S = N$  [or vice versa] is given by the minimum of the marginal stability curve  $\text{Ra}_{\text{stab}}(k; N)$  [or  $N_{\text{stab}}(k; \text{Ra})$ , respectively] with respect to the wave number  $k$ . Without magnetic fields, i.e.,  $N_S = 0$ , the critical values are  $\text{Ra}_c^0 = 27\pi^4/4$ ,  $k_c^0 = \pi/\sqrt{2}$  for IBC, and  $\text{Ra}_c^0 \approx 1707.762$ ,  $k_c^0 \approx 3.116$  for RBC. Applying a static magnetic field, i.e.,  $N_S > 0$ , the curvature of the potential is reduced and the critical Rayleigh number decreases with increasing  $N_S$ , whereas the critical wave number increases [9,20].

### B. Modulated magnetic fields ( $H_M \neq 0$ )

If the applied magnetic field is periodically modulated, i.e.,  $H_M \neq 0$ , the potential  $V$  Eq. (3.3) is periodic, too, and the criteria for determining the stability boundary can be determined with the help of the Floquet theory [21]. According to the Floquet theory the general solution of Eq. (3.2) reads

$$\theta(t) = A e^{(\mu - \Gamma/2)t} P(t) + B e^{(-\mu - \Gamma/2)t} P(-t) \quad (3.6)$$

where  $A$  and  $B$  are determined by the initial conditions.  $P(t)$  is a periodic function with the same period as the potential  $V(t)$  Eq. (3.3), and  $\mu = \mu_r + i\mu_i$  is the complex Floquet exponent, which is a function of the system parameters and of the considered perturbation. After eliminating the damping term  $\Gamma \dot{\theta}$  in Eq. (3.2) via the substitution

$$\theta(t) = y(t) e^{-\Gamma t/2}, \quad (3.7)$$

we integrated the resulting differential equation for  $y$  numerically, using a Runge-Kutta scheme, and calculated  $\mu$  following the method described in [21].

As a result, we get the Floquet exponent as a function of, e.g., the control parameters  $\epsilon$  and  $N_M$  (and fixed remaining parameters). The regions of growth of the variable  $y(t)$  have the form of the well-known Mathieu tongues. The latter are connected with the  $\epsilon$  axis at points  $\epsilon_n^*$  so that resonant driving is possible for an infinitesimal modulation amplitude ( $\propto N_M$ ), if the eigenfrequency ( $\propto \epsilon$ ) of the unmodulated system, i.e., for  $N_M = 0$ , is an integer multiple of half of the modulation frequency. However, the stability boundaries for

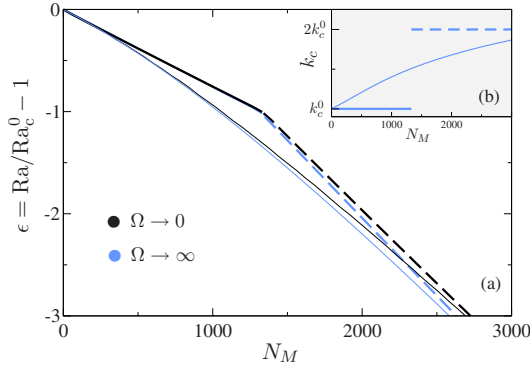


FIG. 2. (Color online) Stability boundaries of the quiescent fluid for high (blue) and low (black) frequency modulation, respectively. Thin lines in (a) show the critical reduced Rayleigh number  $\epsilon = \text{Ra}/\text{Ra}_c^0 - 1$  as a function of  $N_M$  for IBC and thick lines refer to the marginal stability boundaries for  $k = k_c^0$  (full lines) and  $2k_c^0$  (dashed lines), respectively, both for harmonic response. The inset (b) shows the critical (thin line) and the marginal (thick lines) wave number as a function of  $N_M$ .

the physically relevant amplitude  $\theta(t)$  belonging to subharmonic or harmonic resonance are detached from the  $\epsilon$  axis, because the growth rate of  $y(t)$  is reduced by the exponential  $e^{-t\Gamma/2}$ .

By means of a perturbation analysis, an upper boundary for the connection points  $\epsilon_n^*$  for  $y$  and consequential a boundary for the regions of resonance for  $\theta$  can be determined analytically

$$\epsilon_n^* < -\frac{(1 + \text{Pr})^2}{4 \text{Pr}}. \quad (3.8)$$

For large Prandtl numbers  $\epsilon_n^*$  is proportional to  $-\text{Pr}$ , indicating that subharmonic response can only be achieved for large negative  $\epsilon$ . Because large Prandtl numbers are typical for ferrofluids (see for example Table 1 in [13]), harmonic response is to be expected in experiments.

In the following, we discuss the results of the linear stability analysis in detail for a Prandtl number of  $\text{Pr}=50$ , which is used throughout the rest of this paper. In the Appendix, we consider the case of a small Prandtl number ( $\text{Pr}=5$ ) to demonstrate the possibility of subharmonic response appearing already for relatively small negative  $\epsilon$ .

### C. Results

Figure 2(a) shows the linear stability boundaries of the conductive state in the  $\epsilon$ - $N_M$  plane for a Prandtl number of  $\text{Pr}=50$ . The thin black (blue) line indicates the critical reduced relative Rayleigh number  $\epsilon = \text{Ra}/\text{Ra}_c^0 - 1$  as a function of the magnetic Rayleigh number  $N_M$  in the case of the low-(high-)frequency limit  $\Omega \rightarrow 0$  ( $\Omega \rightarrow \infty$ ) of the modulation. The stability boundaries for intermediate frequencies lie in between these limiting cases. Note that for  $\epsilon < -1$  the layer is heated from above and thus it is thermally stabilized. By decreasing the modulation frequency the curves shift toward the black line, i.e., the conductive solution gets stabilized in that case. The corresponding critical wave number  $k_c$  [inset

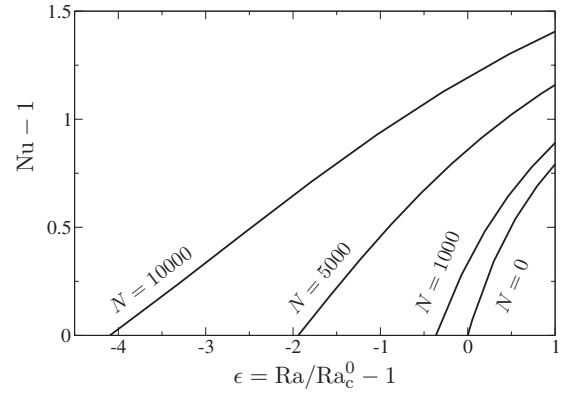


FIG. 3. Bifurcation of the Nusselt number  $\text{Nu}-1$  for RBC as a function of the relative reduced Rayleigh number  $\epsilon = \text{Ra}/\text{Ra}_c^0 - 1$  for stationary magnetic fields. Their strength is labeled by the magnetic Rayleigh numbers from  $N=0$  (no magnetic field) up to  $N=10000$ . Their wave number is in each case the critical one,  $k_c(N)$ .

(b)] starts at  $k_c^0$  in the absence of magnetic fields and increases monotonically with growing magnetic field. The imaginary part of the Floquet exponent is zero at the stability boundaries of Fig. 2, yielding harmonic response. In the high-frequency limit, solely the time average of  $N(t)$  affects the stability behavior. Thus, in this limit the stability boundary coincides with the stationary stability boundary when one uses the mean magnetic Rayleigh number

$$\langle N(t) \rangle = N_M \langle [1 + \cos(\Omega t)]^2 \rangle = 1.5 N_M \quad (3.9)$$

as the control parameter.

To compare with the numerical simulation of the full nonlinear equations, we included in Fig. 2 the stability boundaries only for the discrete wave numbers that are compatible with the lateral periodicity  $\lambda = 2\pi/k_c^0$  of our simulation cell. In the parameter range shown in Fig. 2 only perturbations with wave numbers  $k_c^0$  (full thick lines) and  $2k_c^0$  (dashed thick lines) are able to grow.

## IV. NONLINEAR CONVECTION

In this section we discuss relaxed nonlinear convective states in the form of straight parallel rolls. Thereto the field equations were solved in a vertical cross section through the convection rolls perpendicular to their axes, thus ignoring effects that come from field variations along the roll axes. We used a finite difference method, that is based on the MAC method [22,23]. First we discuss results for stationary driving (Sec. IV A), then for periodic modulation of the magnetic field (Sec. IV B). The simulations were made for the realistic RBC case.

### A. Stationary magnetic fields ( $H_M=0$ )

The Figs. 3 and 4 show bifurcation diagrams of the Nusselt number  $\text{Nu}-1$  for the unmodulated case: (i) in Fig. 3 as a function of the reduced relative Rayleigh number  $\epsilon$  for the fixed magnetic Rayleigh numbers  $N=0, 1000, 5000, 10000$ , and (ii) in Fig. 4(b) as a function of  $N$  for fixed  $\epsilon=0, -1.8$ .

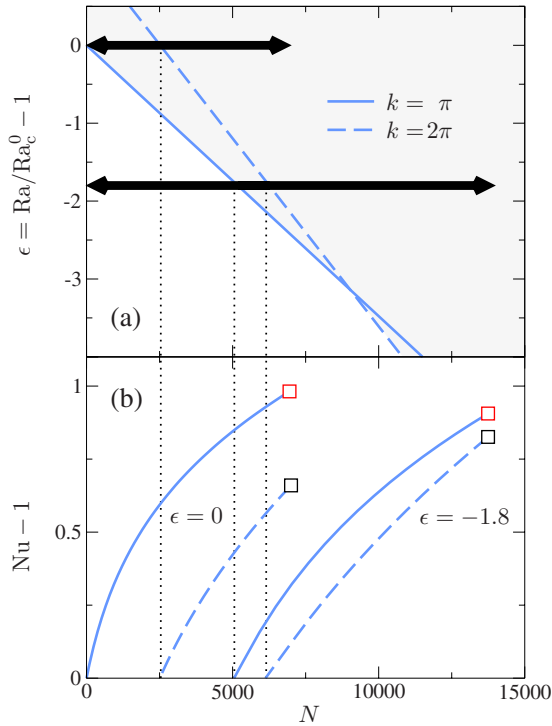


FIG. 4. (Color online) Blue lines in (a) show stationary stability boundaries of the conductive state against the growth of ( $k=\pi$ ) and ( $k=2\pi$ ) perturbations in the  $\epsilon$ - $N$  plane for RBC. The black arrow at  $\epsilon=0$  ( $\epsilon=-1.8$ ) marks the interval over which  $N(t)=N_M [1+\cos(\Omega t)]^2$  varies for  $N_M=1747$  ( $N_M=3494$ ). The bifurcation branches of the Nusselt number  $Nu-1$  for stationary magnetic fields as a function of the magnetic Rayleigh number  $N$  are shown for later reference in (b). The leftmost [rightmost] curves belong to  $k=\pi$  (full line with a red square) and to  $k=2\pi$  (dashed line with a black square), respectively, at  $\epsilon=0$  [ $\epsilon=-1.8$ ], as indicated by the black dotted lines.

We will first discuss the case (i). Here, the periodicity of the simulation cell has been adapted to the associated critical wavelength  $k_c=k_c(N)$ . It increases monotonically with the magnetic Rayleigh number  $N$ , starting with  $k_c(0)\approx 3.12$  in the absence of magnetic fields, and being  $\approx 4.79$  for  $N=10000$ . The bifurcation threshold is shifted to lower  $\epsilon$  values when increasing  $N$ . Below  $\epsilon=-1$ , the fluid is heated from above and cooled from below. But the thermally induced density stratification of the fluid layer can be outbalanced by the Kelvin force, leading to convection. Note that the initial slope of the forward bifurcating Nusselt number curve decreases with increasing  $N$ . The initial slopes are in good agreement with results from a weakly nonlinear analysis [20].

In case (ii) the periodicity of the simulation cell has been fixed to  $\lambda=2$ . The corresponding wave number is  $k=\pi\approx k_c^0$ . Figure 4(a) shows the stationary bifurcation thresholds for perturbations with the wave number  $k=\pi$  (blue solid line) and  $k=2\pi$  (blue dashed line). In Fig. 4(b) the associated bifurcations of  $Nu-1$  are shown as a function of the static magnetic Rayleigh number  $N$  for  $\epsilon=0$  (the two left curves) and  $\epsilon=-1.8$  (the two right curves). Red [black] squares mark the solution branch bifurcating at the ( $k=\pi$ ) threshold [ $k=2\pi$ ] threshold]. These solutions are used later on as a

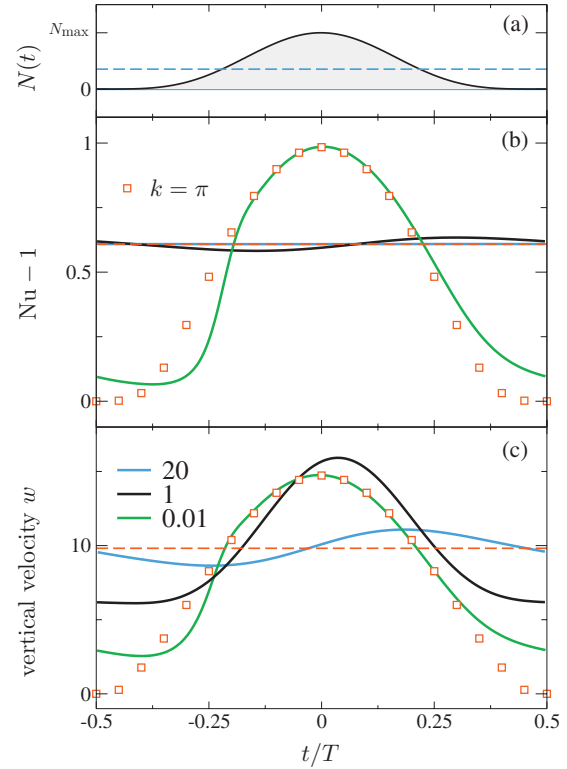


FIG. 5. (Color) Temporal oscillations of (a) the control parameter  $N(t)=N_M[1+\cos(\Omega t)]^2$  ( $N_{\max}=4N_M=6988$ ,  $\epsilon=0$ ), (b) the Nusselt number  $Nu-1$ , and (c) the vertical velocity  $w$  as a function of the reduced time  $t/T$  with  $T=2\pi/\Omega$  being the modulation period.  $w$  is evaluated at midheight between two adjacent rolls. In the legend the respective modulation frequency is given as the multiple of the reference frequency  $\Omega_R$  explained in the text. The red squares show the stationary  $k=\pi$  response to stationary magnetic fields with magnetic Rayleigh number  $N$  given by the actual value of  $N(t)$  in (a). The dashed red lines show the order parameter for stationary driving with the mean magnetic Rayleigh number  $\langle N(t) \rangle = 1.5N_M$ . The full (dashed) blue line in (a) marks the stationary bifurcation threshold for  $k=\pi$  ( $k=2\pi$ ).

basis for comparison with the response to low-frequency modulation.

## B. Modulated magnetic fields ( $H_M \neq 0$ )

In this section we consider the response to periodic modulation of the magnetic field. We investigate the temporal oscillations of the Nusselt number and of the vertical velocity of relaxed nonlinear convective states.

We deal with the case  $H_S=H_M \neq 0$  for the parameter combinations ( $\epsilon=0$ ,  $N_M=1747$ ) and ( $\epsilon=-1.8$ ,  $N_M=3494$ ). The interval over which the magnetic Rayleigh number  $N(t)$  varies is illustrated in Fig. 4(a) by the black double arrows. With respect to the stationary bifurcation thresholds, the magnetic control parameter  $N(t)=N_M[1+\cos(\Omega t)]^2$  is always (partially) in the unstable region for  $\epsilon=0$  ( $\epsilon=-1.8$ ).

### 1. Case $\epsilon=0$

We first discuss the case  $\epsilon=0$ . Figure 5(a) shows the oscillations of the control parameter  $N(t)$ . The stationary bifur-

cation thresholds of  $N$  for  $k=\pi$  (solid blue line) and  $k=2\pi$  (dashed blue line) are included for the sake of reference as well. Figure 5(b) shows the Nusselt number  $Nu-1$ , and (c) the vertical velocity  $w$  as a function of the reduced time  $t/T$  with  $T=2\pi/\Omega$  being the associated modulation period.  $w$  is evaluated at midheight between two adjacent rolls. The temporal oscillations are shown for three different frequencies, namely,  $20\Omega_R$  (blue curves),  $\Omega_R$  (black curves), and  $0.01\Omega_R$  (green curves). Here  $\Omega_R \approx 2\pi/\tau_{\text{vis}}$  is the reference frequency corresponding approximately to one viscous diffusion time  $\tau_{\text{vis}}=d^2/\nu$ . For comparison, the constant values for stationary driving with the mean  $\langle N(t) \rangle = 1.5N_M$  as control parameter (red dashed lines), as well as the values for the stationary solution branch that bifurcates at the stability threshold for  $k=\pi$  (red squares) are included.

The results are as follows: for the modulation with the high frequency  $20\Omega_R$ , the dynamics of the convection is nearly averaged, e.g., the oscillation amplitude of the Nusselt number is small compared to its mean value (b). The modulation amplitude of the velocity field is barely  $\approx 12\%$  of its time mean (c). A phase shift between the maximum of  $N$  and the maximum of the velocity  $w$  or the Nusselt number  $Nu$  occurs: the latter ones are temporally delayed to the former because of the inertia of the fluid resisting the fast changing accelerating Kelvin force leading to this time lag. Consistently the phase shift decreases with decreasing frequency. That is best seen for the velocity profiles in (c). Thereby the oscillation amplitudes are increasing and the oscillation profiles become more anharmonic. The lower the modulation frequency, the closer the oscillation profiles get to the curve displayed by the red squares. Deviations just persist in the vicinity of the bifurcation threshold, because the dynamics become infinitely slow there.

## 2. Heating from above

We now discuss the case  $\epsilon=-1.8$ . The high-frequency behavior is shown in Fig. 6 and the low frequency one in Fig. 7. The setup of these figures is the same as in Fig. 5 (cf. last paragraph). In contrast to the previous case of  $\epsilon=0$ , the magnetic Rayleigh number now *crosses* periodically the stationary bifurcation threshold (cf. the lower double arrow in Fig. 4). This affects particularly the low frequency behavior.

*High-frequency behavior*—The high-frequency behavior is basically the same as for  $\epsilon=0$ , i.e., the oscillation amplitude decreases and the phase shift increases with increasing modulation frequency, approaching the respective values for  $Nu$  and  $w$  for stationary driving with the mean  $\langle N(t) \rangle = 1.5N_M$  as control parameter (red dashed lines). But in the present case two exceptions are worth mentioning: (i) the mean of, e.g., the Nusselt number increases and (ii) the sense of rotation of the convection rolls changes periodically for frequencies lower than  $\approx 10\Omega_R$ . Here, the increase in the mean Nusselt number is due to the shift of the stability boundary [cf. Fig. 2(a)], leading to a larger distance from the bifurcation threshold for increasing modulation frequency. On the other hand, the change of the sense of rotation is due to the restoring thermal buoyancy force (heating from above) that causes the stabilization of the conductive solution. And the inertia of the fluid leads to an overshooting.

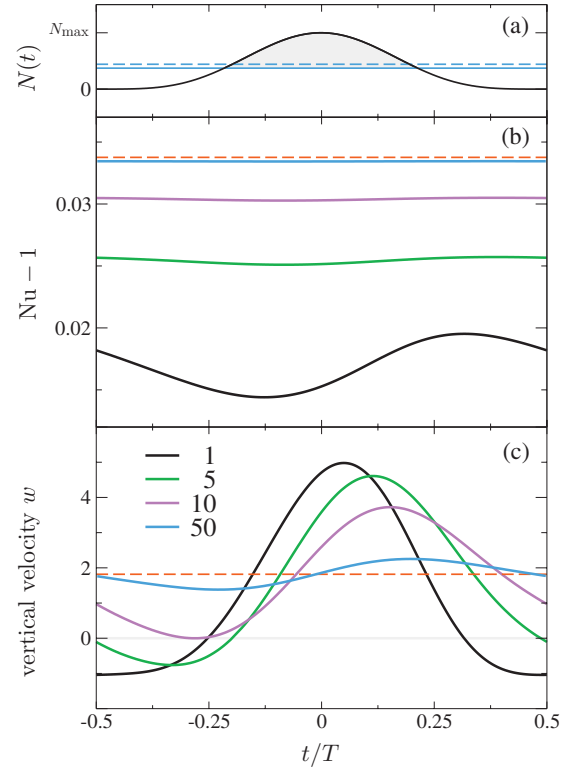


FIG. 6. (Color) Temporal oscillations of (a) the control parameter  $N(t) = N_M[1 + \cos(\Omega t)]^2$  ( $N_{\text{max}} = 4N_M = 13976$ ,  $\epsilon = -1.8$ ), (b) the Nusselt number  $Nu-1$ , and (c) the vertical velocity  $w$  as a function of the reduced time  $t/T$  with  $T = 2\pi/\Omega$  being the modulation period.  $w$  is evaluated at midheight between two adjacent rolls. In the legend the respective modulation frequency is given as the multiple of the reference frequency  $\Omega_R$ . The dashed red lines show the order parameters for stationary driving with the mean magnetic Rayleigh number  $\langle N(t) \rangle = 1.5N_M$ . Note, that for frequencies  $\Omega \lesssim 10\Omega_R$  the sense of rotation changes. The full (dashed) blue line in (a) marks the stationary bifurcation threshold for  $k=\pi$  ( $k=2\pi$ ).

*Low-frequency behavior*—The low-frequency behavior is shown in Fig. 7 for  $\Omega/\Omega_R = 0.015$  (black),  $5 \cdot 10^{-3}$  (green),  $1 \cdot 10^{-3}$  (magenta), and  $1 \cdot 10^{-4}$  (blue). For comparison, the values for the stationary solution branches bifurcating at the stability thresholds for  $k=\pi$  (red squares), and for  $k=2\pi$  (black squares), respectively, are included. The lower the modulation frequency, the larger the oscillation amplitudes, thereby approaching the limiting value given by the respective stationary solution curve. For intermediate frequencies, here shown for  $\Omega/\Omega_R = 5 \cdot 10^{-3}$  (green), and  $1 \cdot 10^{-3}$  (magenta), a fast growth of the amplitude followed by a pronounced overshooting can be observed, relaxing just similarly fast to values close to the stationary ones belonging to the curve bifurcating at the ( $k=2\pi$ ) threshold (black squares). For low enough frequencies, here demonstrated for the case  $\Omega/\Omega_R = 1 \cdot 10^{-4}$  (blue), the time interval, where  $N(t)$  is overcritical with respect to the ( $k=\pi$ )-threshold, but still undercritical with respect to the ( $k=2\pi$ )-threshold, suffices for a ( $k=\pi$ ) perturbation to become large enough that a ( $k=2\pi$ ) perturbation, starting to grow later, cannot compete. Hence, the oscillation profiles for very low frequencies approach the stationary  $k=\pi$  curve (red squares).

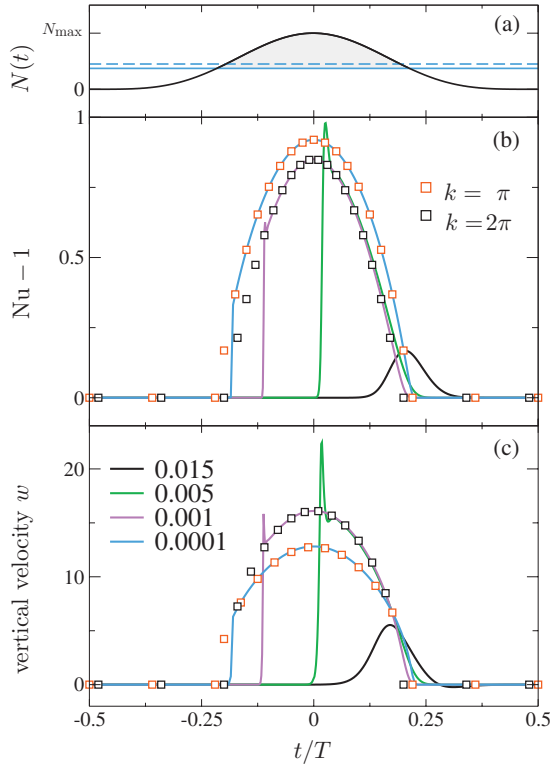


FIG. 7. (Color) Temporal oscillations of (a) the control parameter  $N(t) = N_M [1 + \cos(\Omega t)]^2$  ( $N_{\max} = 4N_M = 13976$ ,  $\epsilon = -1.8$ ), (b) the Nusselt number  $Nu-1$ , and (c) the vertical velocity  $w$  as a function of the reduced time  $t/T$  with  $T = 2\pi/\Omega$  being the modulation period.  $w$  is evaluated at midheight between two adjacent rolls. In the legend the respective modulation frequency is given as the multiple of the reference frequency  $\Omega_R$ . The red (black) squares show the stationary  $k = \pi$  ( $k = 2\pi$ ) response to stationary magnetic fields with magnetic Rayleigh number  $N$  given by the actual value of  $N(t)$  in (a). The full (dashed) blue line in (a) marks the stationary bifurcation threshold for  $k = \pi$  ( $k = 2\pi$ ).

### 3. Effect of noise for small $\Omega$

The results obtained by the numerical simulations for low-frequency modulation has to be taken with care, because numerical noise prevents the field amplitudes to become as small as they should do in the undercritical phase of driving. Instead, the noise level, depending on the numerical accuracy, provides a lower bound for the convective field amplitudes below which they cannot decrease. This is illustrated by Fig. 8. We have chosen the temporal evolution of the dominant lateral Fourier coefficients  $\hat{w}_1$  (full line) and  $\hat{w}_2$  (dashed line) of the lateral velocity profile of  $w$  in the middle of the layer as characteristics to demonstrate the influence of the numerical noise on the stability behavior and on the pattern selection. For  $\Omega/\Omega_R = 0.015$  [black curves in (b)],  $\hat{w}_1$  is dominant during the whole period, while  $\hat{w}_2$  is always several orders of magnitude smaller. Hence,  $\hat{w}_2$  is not influencing the solution, although its value cannot fall below  $\approx 10^{-16}$  in the undercritical phase of driving due to numerical noise. The situation changes already for a slightly smaller modulation frequency: For  $\Omega/\Omega_R = 0.01$  [red curves in (b)],  $\hat{w}_2$  can grow to much higher values thereby influencing the structure

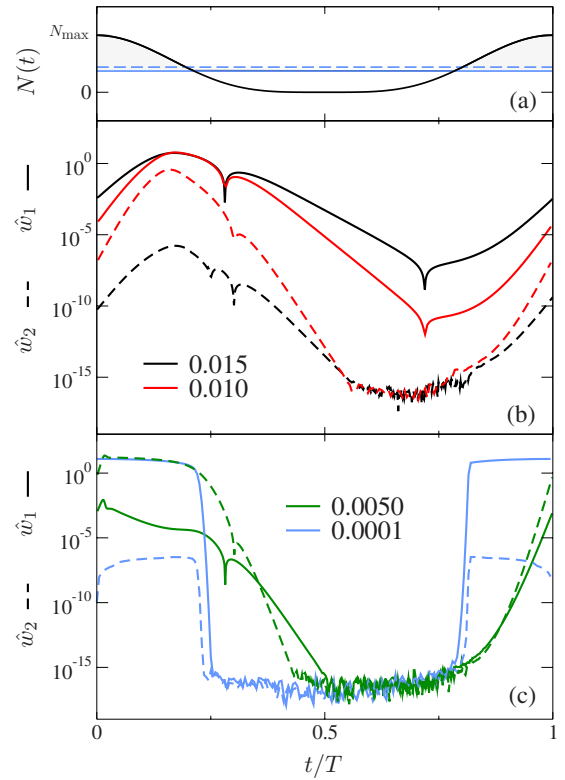


FIG. 8. (Color online) Temporal oscillations of (a) the control parameter  $N(t) = N_M [1 + \cos(\Omega t)]^2$  ( $N_{\max} = 4N_M = 13976$ ,  $\epsilon = -1.8$ ), and (b), (c) the first two Fourier modes  $\hat{w}_1$  and  $\hat{w}_2$  of the lateral velocity profile  $w$  at midheight as a function of the reduced time  $t/T$  with  $T = 2\pi/\Omega$  being the associated modulation period. In the legend the respective modulation frequency is given as the multiple of the reference frequency  $\Omega_R$ . The Fourier modes cannot fall below  $\approx 10^{-16}$  in the undercritical phase of driving [concerning to the stationary stability boundaries, see (a)] due to numerical noise.

significantly. In fact, the resulting oscillations are not strictly periodic anymore. The maximum value of  $\hat{w}_2$  differs from one cycle to another, because it starts growing out of a noise induced random value in the overcritical phase of driving. Increasing the modulation period further, here shown for  $\Omega/\Omega_R = 0.005$  and  $0.0001$ , both  $\hat{w}_1$  and  $\hat{w}_2$  are noise influenced. For  $\Omega/\Omega_R = 0.005$  [green (dark gray) curve in (c)],  $\hat{w}_2$  becomes the dominant mode, while for  $\Omega/\Omega_R = 0.0001$  [blue (light gray) curve in (c)],  $\hat{w}_1$  dominates.

The presence of noise consequently leads to the fact, that—strictly speaking—convection appears always provided that (i) the stationary bifurcation threshold is crossed during one cycle, and (ii) the modulation period is large enough, depending on the magnitude of the noise level. In fact, this is not really a restriction, because in experiments perturbations, that are orders of magnitudes larger than the numerical noise in the simulations, are always present. However, one can include the perturbations that characterize the specific experimental situation also in the numerical simulations in order to obtain results that are suitable for comparing with these experiments.

V. SUMMARY

We have investigated the linear stability and the nonlinear convective properties of a ferrofluid in the Rayleigh-Bénard geometry, exposed to a constant vertical temperature gradient and a temporal periodic but spatially homogeneous external magnetic field normal to the fluid layer. The ferrofluid is regarded as a one component magnetizable fluid. Its magnetization is equilibrated at every time instant and it is only a function of the magnetic field and of the temperature. The magnetic driving enters the momentum balance equation via the Kelvin force density, which is periodic in our case. It turns out that the linear stability properties of the quiescent conductive state are captured by the growth behavior of parametrically driven harmonic oscillators. The stability of the conductive state and particularly the type of response, which can be harmonic or subharmonic, is determined by the system parameters. The stability boundary of the conductive state in the high-frequency limit coincides with the stationary stability boundary if one uses a mean magnetic Rayleigh number. The stability boundary for low-frequency modulation is shifted in a way that the conductive state gets stabilized. We found, that subharmonic response is not typical for ferrofluids because of their high Prandtl numbers. But in low-Prandtl number simulations we found nonlinear relaxed subharmonic convective states as predicted by the linear analysis.

The nonlinear response has been investigated for heating from below and from above for a large span of modulation frequencies. For high-frequency modulation the dynamics is nearly averaged and the order parameters approach the values which they have for a driving with the corresponding mean magnetic Rayleigh number. In the case of heating from above, a change in the sense of rotation of the convection rolls has been observed that is due to the stabilizing thermal restoring force and to the inertia of the fluid, leading to an overshooting. We have seen that for low-frequency modulation the numerical noise can influence the pattern selection. This is the case, if the convection amplitudes cannot go below the noise level, depending on the numerical accuracy, in the undercritical phase of driving. The simulations showed that for very low modulation frequencies the oscillation profiles approach the stationary curves.

ACKNOWLEDGMENT

This work was supported by the Deutsche Forschungsgemeinschaft.

APPENDIX: SUBHARMONIC RESPONSE

Although large Prandtl numbers are typical for ferrofluids, we show here also a stability map for a small Prandtl number of  $Pr=5$  and  $\Omega=0.2\Omega_R$  to demonstrate the possibility of subharmonic response appearing for relatively small negative  $\epsilon$  in that case. Thereto, we considered the growth behavior of lateral periodic perturbations of the temperature deviation  $\theta$  with periodicity length  $\lambda=2\pi/k_c^0$ ,  $k_c^0=\pi/\sqrt{2}$  being the critical wave number for IBC in the absence of a magnetic field. The stability boundaries of the conductive state against the

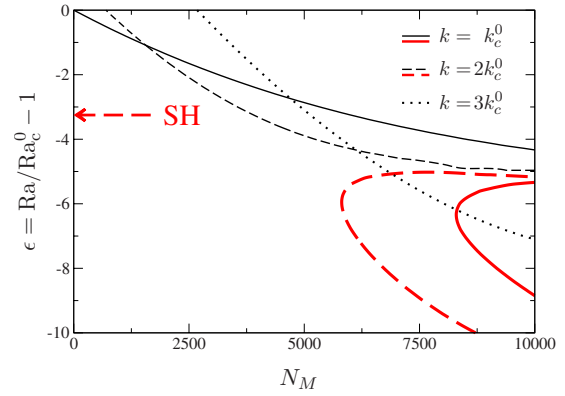


FIG. 9. (Color online) Stability boundaries of the conductive state against the growth of  $\theta_{m1}$  modes in the  $\epsilon-N_M$  plane for  $Pr=5$  and  $\Omega=0.2\Omega_R$ . Solid, dashed and dotted lines correspond to  $m=1$ ,  $m=2$  and  $m=3$ , respectively. Black (red) lines are related to harmonic (subharmonic) response. The red arrow marks  $\epsilon_1^*$  of the first subharmonic response of  $y$  [see Eq. (3.7)] associated to the  $\theta_{21}$  mode.

growth of different  $\theta$  modes are shown in Fig. 9 in the plane spanned by the control parameters  $\epsilon$  and  $N_M$ . For the presented parameter range, only a few modes get unstable— $\theta_{11}$  (solid line),  $\theta_{21}$  (dashed line), and  $\theta_{31}$  (dotted line)—, starting to grow harmonically (subharmonically) beyond the respective black (red) curve in the unstable region. The type of response is determined by the associated imaginary part of the Floquet exponent, which is 0 ( $\pi/T$ ) by crossing the black (red) curves. The red arrow marks the connection point  $\epsilon_1^*$  [ $<-1.8$ , see Eq. (3.8)] of the domain of first subharmonic resonance of  $y$  associated to the  $\theta_{21}$  mode.

To demonstrate subharmonic resonance, we have chosen an appropriate parameter combination for RBC:  $\epsilon=-5.5$  and  $N_M=13000$ . Figure 10 shows the subharmonic response of a relaxed nonlinear state by displaying the temporal oscillations of the vertical velocity  $w$  [black line, (b)] and the temperature deviation  $\theta=\delta T-\delta T_{\text{cond}}$  [red line, (b)] at midheight between two adjacent rolls for two periods of modulation.

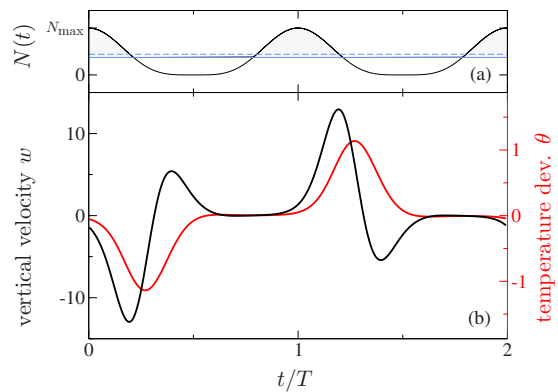


FIG. 10. (Color online) Subharmonic response displayed by temporal oscillations of (b) the vertical velocity  $w$  (black line) and the temperature deviation  $\theta=\delta T-\delta T_{\text{cond}}$  (red line) at midheight between two adjacent rolls for two periods of the modulation. The magnetic Rayleigh number  $N(t)=N_M[1+\cos(\Omega t)]^2$  is shown in (a). Parameters are  $Pr=5$ ,  $\epsilon=-5.5$ ,  $N_M=13000$ , and  $\Omega=0.2\Omega_R$ .

The magnetic Rayleigh number  $N(t) = N_M [1 + \cos(\Omega t)]^2$  is shown in (a). Therein, the blue solid (dashed) line marks the stationary bifurcation threshold for  $k = \pi$  ( $k = 2\pi$ ). There occurs a phase shift between the maximum of the driving  $N$ , e.g., at  $t/T = 1$  ( $t/T = 0$ ), and the maxima (minima) of the velocity  $w$  and the temperature deviation  $\theta$ : the latter ones are temporally delayed to the former. For the subharmonic response, that leads to  $f(t) = f(t + 2T)$  with  $f$  representing an

arbitrary field variable, one observes the following additional temporal symmetry

$$f(z, t) = \mp f(-z, t + T). \quad (\text{A1})$$

Here the minus (plus) sign holds for  $f = \delta T$  and  $w$  ( $f = u$  and  $\Phi$ ). This symmetry can easily be seen by comparing, e.g., the absolute values of the field extrema in Fig. 10(b).

- 
- [1] M. C. Cross and P. C. Hohenberg, *Rev. Mod. Phys.* **65**, 851 (1993).
- [2] E. Bodenschatz, W. Pesch, and G. Ahlers, *Annu. Rev. Fluid Mech.* **32**, 709 (2000).
- [3] G. Venezian, *J. Fluid Mech.* **35**, 243 (1969).
- [4] P. M. Gresho and R. L. Sani, *J. Fluid Mech.* **40**, 783 (1970).
- [5] G. Ahlers, P. C. Hohenberg, and M. Lücke, *Phys. Rev. A* **32**, 3493 (1985).
- [6] G. Ahlers, P. C. Hohenberg, and M. Lücke, *Phys. Rev. A* **32**, 3519 (1985).
- [7] J. L. Neuringer and R. E. Rosensweig, *Phys. Fluids* **7**, 1927 (1964).
- [8] R. E. Rosensweig, *Ferrohydrodynamics* (Cambridge University Press, London, 1985).
- [9] B. A. Finlayson, *J. Fluid Mech.* **40**, 753 (1970).
- [10] L. Schwab, U. Hildebrandt, and K. Stierstadt, *J. Magn. Magn. Mater.* **39**, 113 (1983); L. Schwab, Ph.D. thesis, Ludwig-Maximilians-Universität München, 1989 (unpublished).
- [11] J. Huang, B. F. Edwards, and D. D. Gray, *Phys. Fluids* **9**, 1819 (1997).
- [12] J. Huang, D. D. Gray, and B. F. Edwards, *Phys. Rev. E* **57**, 5564 (1998).
- [13] P. N. Kaloni and J. X. Lou, *Phys. Rev. E* **70**, 026313 (2004).
- [14] P. N. Kaloni and J. X. Lou, *Phys. Rev. E* **71**, 066311 (2005).
- [15] S. Aniss, M. Belhaq, and M. Souhar, *ASME J. Heat Transfer* **123**, 428 (2001).
- [16] L. D. Landau and E. M. Lifshitz, *Fluid Mechanics* (Pergamon Press, London, 1987).
- [17] L. D. Landau and E. M. Lifshitz, *Electrodynamics of Continuous Media* 2nd ed. (Pergamon Press, London, 1989).
- [18] R. E. Rosensweig, *J. Chem. Phys.* **121**, 1228 (2004).
- [19]  $\nu = \eta / \rho$  with the effective viscosity  $\eta$ , which is the sum of the pure fluids viscosity and the rotational viscosity.
- [20] A. Recktenwald and M. Lücke, *J. Magn. Magn. Mater.* **188**, 326 (1998).
- [21] M. Abramowitz and I. A. Stegun, *Handbook of Mathematical Functions* (Dover, New York, 1965).
- [22] C. W. Hirt, B. D. Nichols, and N. C. Romero, Technical Report LA-5852, Los Alamos Scientific Lab., N. Mex. (USA), 1975.
- [23] F. H. Harlow and J. E. Welch, *Phys. Fluids* **8**, 2182 (1965).